

# Investigation of photocurrent and recombination dynamics of photodiodes based on polymeric materials

GUILIN LIU\*, JIANBO SHAO, XIAO WANG YIQING ZHU, WEIYING QIAN, GUOHUA LI  
*School of Science, Jiangnan University, Wuxi 214122, China*

Organic photodiodes (OPD) based on P3HT:PCBM bulk heterojunction were fabricated and characterized under different voltage bias. The photodiodes demonstrated a stable signal around specified wavelength at 550 nm under a reverse bias at -2.5V, showing a potential application for specific wavelengths detection. The photocurrent responsivity indicated that free charge carriers can be extracted within microseconds after the light cut-off. The periodic time was about 2  $\mu$ s (fastest was 1.5  $\mu$ s under high intensity condition) under different light intensity. The transient technique was applied to investigate the recombination rate inside of organic photodetector in order to elucidate the dominant decay mechanism. The mobility and charge carrier density values obtained with transient absorption spectrum show a result of geminate recombination after exciton separation being the dominant loss mechanism. Although the process was dominated by recombination, OPD worked perfectly in low light condition indicating a potential application in sensing market.

(Received March 20, 2017; accepted November 28, 2017)

*Keyword:* Organic Photodetector, Photocurrent, Transient technique

## 1. Introduction

Organic semiconductors have been investigated for decades [1-5] and now their presence in many different applications is growing rapidly [6]. Organic semiconductor devices are showing a niche in light detection field based on advantages such as flexibility [7, 8], tuned color [9] and large area coverage [10]. This area is up to date dominated by silicon-based technology with offers faster responsivity [11], higher reliability [12] and better Signal-Noise Ratio (SNR) [13]. Though organic semiconductors are increasing attentions to other optoelectronic applications such as photovoltaics [14-17] and Organic Light Emitting Diodes (OLEDs) [18-21], the investigations on organic photodiodes were hardly improved due to both low power conversion efficiency and high dark current effect. Lim et al. [22] and Kim et al. [23] have devoted some efforts to improve the SNR of Organic Photodetectors (OPDs) after being modified by several different buffer layers. The introduction of these layers contributed to significantly the dark current decreasing. In-depth research based on such kind of optimized structures was applied to develop different sensors. Tse [24] devised bulk heterojunction photodiode arrays based on sandwich geometry, which worked properly as an image sensor. On the other hand, the photocurrent output around nanoamps was the biggest disadvantage in his experiments.

Photodiodes are expected to have strong responsivity. However, trade-offs due to problems with photon

absorption and charge recombination require to be balanced. Unlike solar cells, photodiodes usually work with an external electrical field because detection speed is more important for photodiodes [25]. Belen et al. [25] found that OPDs based on P3HT/PCBM heterojunction is feasible to be integrated into high speed sensing systems. However, extracted charges sometimes cannot give logic true under high speed condition. Because the low level current signal is easily buried underneath a dark current. Therefore, the dynamic of charge carriers inside of BHJ is worthy investigated. After photon excitation, de-excitation mechanism is still ambiguous due to stronger coulomb interaction in organic heterojunctions [26, 27].

## 2. Experimental

The photosensitive materials were blends of Poly(3-hexylthiophene-2,5-diyl) (P3HT, Sigma Aldrich) and [6,6]-phenyl-C<sub>61</sub>-butyric acid methyl ester (PCBM, Sigma Aldrich) in 1:1 ratio by weight which had been prepared in chlorobenzene solution (10 mg/ml) 24 hours before the spin coating step. The organic photodiode consisted of 200 nm Indium Tin Oxides (ITO, NanKwong), followed by spin-coating of 30 nm PEDOT: PSS layer and 90 nm BHJ blend respectively. 10 min annealing was then carried out at 135°C in Nitrogen glove box. After the baking process, the top electrode (Aluminum, Kurt J. Lesker) was evaporated by Physical Vacuum Deposition (PVD) system in an atmosphere of 10<sup>-4</sup> Pa.

Organic photodiodes were first characterized in terms of photovoltaic performance in a nitrogen filled glove box after fabrication. The Current Voltage ( $J$ - $V$ ) measurements was carried out with Keithley 2400 source unit under standard solar irradiation (AM1.5, San-EI). Sample was then sealed in glovebox by acrylic glue (K-302, Kafuter) before photocurrent characterization and transient measurements. After the encapsulation and longtime degradation, the photocurrent characterization and the External Quantum Efficiency (EQE) were then measured in ambient via same setup, which consists of a lock-in SR 830, 100 W halogen tungsten lamp, UV 808 Newport U-V enhanced silicon detector and a thotlabs mechanical chopper (219 Hz). Photocurrent response under different applied bias ranging from -2.5 V to 2.5 V were measured, the current amplifier was modulated by the mechanical chopper, where the in-phase photocurrent was signal from light on pulse and out of phase was collected in the light off period, while the EQE was calibrated by the silicon detector (UV 808) without voltage bias based on the same setups of photocurrent. It was worthy emphasized that all samples were kept in ambient long time (over a year) after the encapsulation in order to check the polymer stability. Photocurrent and EQE results were characterized long time after the fabrication.

Transient technique, including Transient Photo Voltage (TPV), Transient Photo Current (TPC) and Transient Absorption Spectrum (TAS), was then characterized in ambient as well. Probing light (970 nm) from a 120 mW LED continuously went through modulated mechanical chopper (219 Hz), a manual beam shutter and a focus lens, finally was focused on the sample which was placed on a homemade sample holder in air. The current and voltage oscillation was monitored by an oscillator, while input signal was both controlled by a function generator and a delay generator. Equilibrium charge carriers were extracted by a linearly increasing voltage ramp generated by the function generator. The generator was also a voltage source for sample and trigger. A 532 nm laser pulse provided a photo excitation as a perturbation. Once the sample was excited by the laser pulse, the laser signal was immediately detected by a photo-diode which triggered the delay generator. The delay time between voltage pulse and light pulse was controlled by the function generator. The open circuit voltage of OPD was lineally increased to 350 mV, 400 mV, 450 mV, 500 mV, 550 mV, respectively by adjusting the pump energy. After the pump irradiation, the probe light after a certain delay time was incident on OPD, then the dynamic of current decay was measured over time.

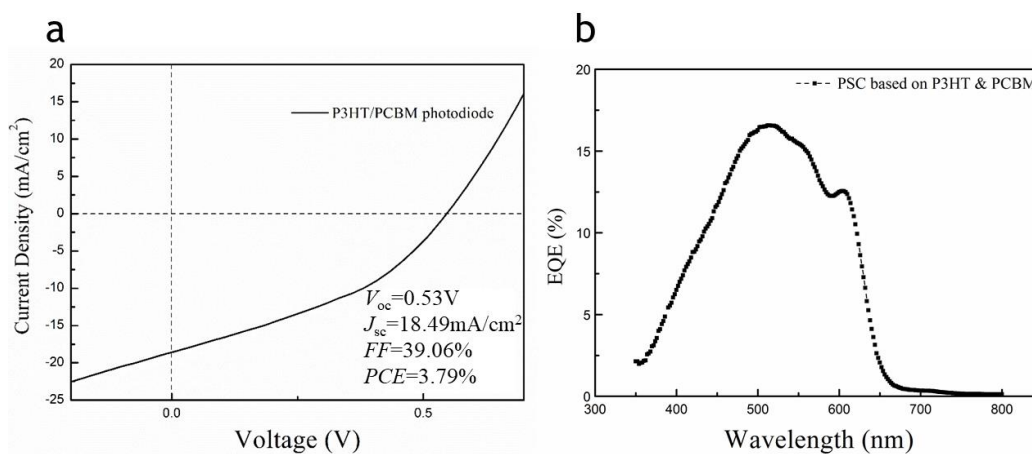


Fig. 1.  $J$ - $V$  characteristic. (a) The power conversion efficiency of OPD under AM 1.5 irradiation condition. (b) The external quantum efficiency was characterized after photocurrent experiments. The  $J$ - $V$  curve was measured immediately after sample fabrication, while the EQE was carried out a year later after been degraded in ambient

### 3. Results and discussion

Fig. 1 shows the ( $J$ - $V$ ) curve and calibrated EQE result of OPD. In Fig. 1 a, the Current Voltage ( $J$ - $V$ ) curve under solar irradiation (AM1.5) was plotted. The OPD showed a strong photocurrent output under illumination without voltage bias. The Power Conversion Efficiency (PCE) achieved almost 4%, with over 0.5 V open circuit voltage. The low FF value of 39% was probably caused by high series resistance ( $R_s=1356.31\Omega$ ). Contrarily to

crystalline Si photodetectors [27], OPDs are not attractive in application due to significant higher  $R_s$ . The  $J$ - $V$  characterization was carried out in glove box, while EQE was measured in ambient over a year after photocurrent and transient experiments. Fig. 1b shows the EQE of device, the maximums appear at 510 nm and secondary shoulder appears at around 610 nm. The photocurrent decreased dramatically after 650 nm, showing photocurrent response range in wavelength from 450 nm to 620 nm. Though OPD has been exposed in air over ten

thousand hours, the EQE was still around 15% at absorption peaks which represented a strong stability. The EQE performance was simultaneously measured in Sunteck<sup>®</sup> lab in order to guarantee the ambient stability, results were coincident with each other. One the other hand, contrasted with instant fabricated devices, EQE performance was relative weaker mainly attributed to higher series resistance. Because of that, geminate recombination rate was significantly increased leading to rapid signal decay, which would be discussed in details in the following TPV-part-discussions. Furthermore, weak photocurrent output could be adjusted in amplified circuit based on guaranteed SNR.

$J$ - $V$  performance was carried out under AM 1.5 irradiation, the output photocurrent was higher over 18 mA/cm<sup>2</sup> which was out of limitation to be applied in sensing circuit. On the other hand, the  $J$ - $V$  curve was measured under extremely high light intensity (1000W/m<sup>2</sup>). In most occasions, OPD was applied in low light or monochromatic condition. The photocurrent spectra under different applied bias ranging from -2.5 V to 2.5 V were obtained and shown in Fig. 2. It can be seen that the in- and out-of-phase components of the photocurrent spectra changed along with the voltage bias. The predominant in-phase component of photocurrent under 2.5 V suggest

fast charge sweep across the device active area and efficiently collected due to superposition of applied and built-in electric fields. Charge carriers under forward bias receive enough energy to escape from traps, reducing charge recombination. Consequently, negligible out-of-phase photocurrent was observed since most carriers were collected already by the time when the light was blocked. The in-phase photocurrent was then decreased as we lowered the forward bias. For -0.5V reverse bias, the in-phase photocurrent component vanished because the built-in electric field was neutralized by the external electric field. When the light was blocked by the chopper, the sample worked like a diode without photo injections as it can be seen from the out of phase photocurrent (Fig. 2 b). As the reverse bias kept growing to -2.5V, the in-phase photocurrent was inverted to negative while the out of phase photocurrent went to positive. It indicated that organic photodetector can work at reversed bias. One important reason is that the out-of-phase current almost close to zero which cannot distinguish out-of-phase signal and background dark current under forward bias. By contrast, sample under reverse bias generated clear signals in both in-phase and out-of-phase conditions.

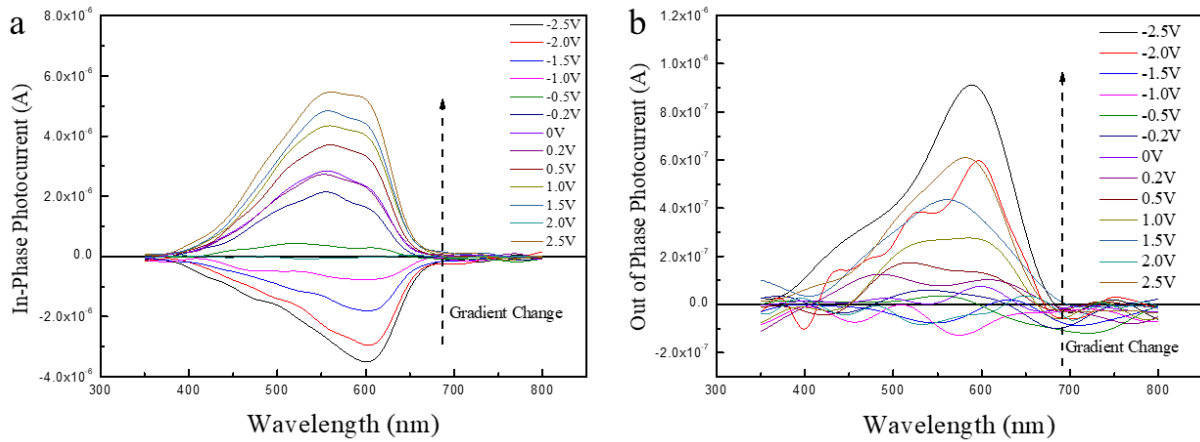


Fig. 2. Photocurrent out put under different voltage biases. The light signal input was modulated by a 219hz optical chopper. (a) shows the in-phase photocurrent under different voltage biases, while (b) is the out-of-phase photocurrent

The photocurrent depends on the decay of the charge carriers over time [30], the mechanism is worthy investigated. According to Shuttle et al. [31] the mono-exponential decay of excited can be written as

$$\frac{d\Delta V}{dt} \propto \frac{d\Delta n}{dt} = -k_{eff}\Delta n = -\frac{\Delta n}{t_{\Delta n}}$$

Where  $\Delta V$  is the photovoltage,  $t$  is the time,  $k_{eff}$  is the pseudo-first-order recombination rate constant,  $\Delta n$  is change in the density of photogenerated carriers due to the pump pulse, and  $t_{\Delta n}$  is the corresponding carrier lifetime. The recombination rate coefficient  $k_{eff}$  depends on the

effective mobility of the charge carriers and geminate recombination factor.

The charge carrier dynamics were represented in Fig. 3. Fig. 3a shows the TAS traces measured with chopped background white light in order to obtain the information of background carrier density. Fig. 3b represents that both the carrier density  $c(t)$  and open circuit volt were monotonously increasing with background illumination intensity in different rates. It was worth mention that the  $c(t)$  is the background carrier density and was calculated from TAS with only chopped background illumination as excitation source and probed by the 970 nm LED light. During the TPC measurements, equilibrium carriers were extracted from devices with a linear reverse bias voltage

ramp (slope  $k=dU/dt$ ). The charge carrier mobility then can be estimated from the time point where the maximum current was measured:  $\mu=2d^2/(3kt_{\max}^2)$ . Where  $d$  is the thickness of sample,  $k$  is the slope of voltage ramp and  $t_{\max}$  equals to the time of maximum carrier extraction. The current signal was traced until the end time point of the extraction. The extracted charge,  $Q_e$ , can be calculated by:

$$Q_e = \int_0^{pulse} \Delta j dt$$

Table 1. Intrinsic parameters of photodetector characterized by transient photo-voltage technique

Pump Energy ( $\mu\text{W}$ )	Transient $V_{oc}$ (mV)	Stationary carrier density ( $\text{cm}^{-3}$ )	Recombination rate ( $\text{cm}^3/\text{s}$ )	Effective mobility ( $\text{cm}^2/\text{V}\cdot\text{s}$ )
28000	550	$2.09 \times 10^{16}$	$1.39 \times 10^{-12}$	$5.44 \times 10^{-4}$
2040	500	$5.46 \times 10^{15}$	$6.64 \times 10^{-13}$	$5.54 \times 10^{-5}$
284	450	$2.52 \times 10^{15}$	$3.92 \times 10^{-13}$	$1.86 \times 10^{-5}$
119	400	$5.95 \times 10^{14}$	$6.46 \times 10^{-13}$	$1.34 \times 10^{-5}$
50	350	$7.29 \times 10^{14}$	$3.01 \times 10^{-13}$	$1.54 \times 10^{-5}$

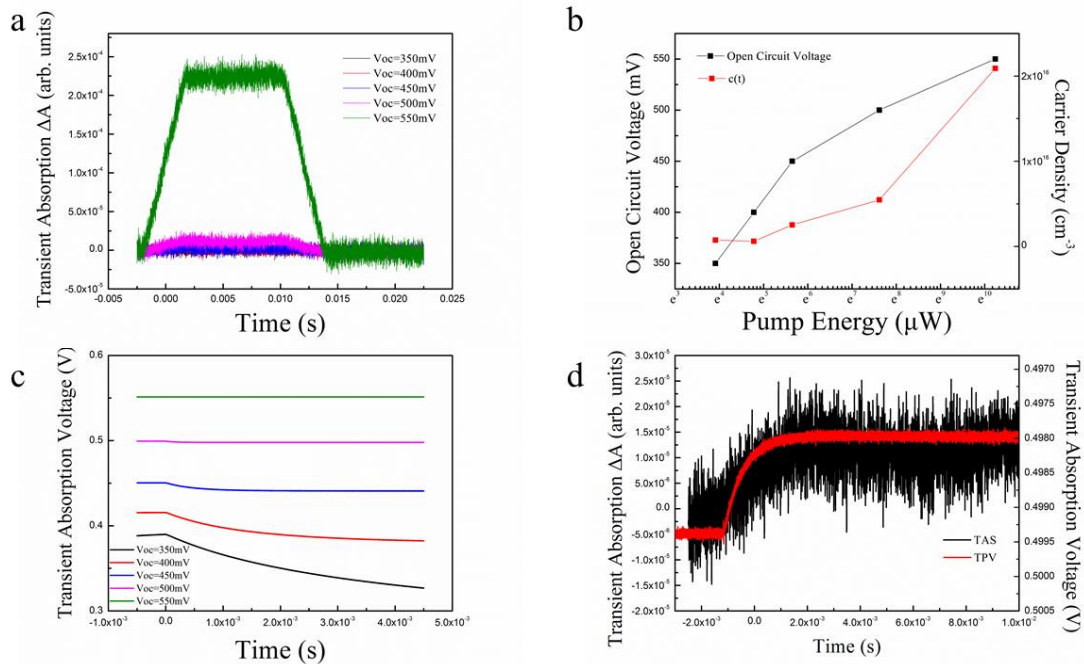


Fig. 3. (a) TAS traces measured only with chopper background illumination to measure the background carrier density. (b) The variation of charge carrier density obtained from TAS and increase in the open circuit voltage obtained from TPV upon increase in the background light intensity. (c) is the TPV curves after photoexcitation under different light intensity. (d) shows the TPV and TAS were coincidence with each other because of geminate recombination

In Fig. 3b, the Open-Circuit Voltage ( $V_{oc}$ ) gradients along with the pump energy was drawn and compared with carrier density. In low light intensity condition,  $V_{oc}$  rapidly increased compares to high light intensity condition. There is a possibility that charge extraction efficiency is higher in low light scenario. Similarly, carrier density increased much slower in weak pump condition contrasted with strong power condition also indicates that most charges in low light condition was rapidly extracted to electrode instead of remaining inside of BHJ. On the other hand, recombined charge carriers mostly occurred

Where  $\Delta j$  is the faradaic current density obtained as the difference between the total current  $j$  and the capacitive current  $j(0)$ , which is assumed to be constant over the whole pulse duration. The charge carrier density  $\rho$  then can be obtained from:  $\rho=Q_e/eSd$ .  $d$  is the thickness of sample and  $e$  is the elementary charge,  $S$  is the electrode area [30, 32]. All parameters were calculated and given in Table 1.

with geminate recombination, because the curves of TAS and TPV perfectly fit with each other as Fig. 3 (d) shows. In TPV condition, the sample was setup in open -circuit condition, where charge carriers could only recombination exists. Meanwhile, the TAS results, though the signal was noisy the TAS showed the same tendency after photons injections, in TAS, both geminate and non-geminate recombination exist.

Aiming to confirm the geminate recombination dominated process, OPD was characterized based on photocurrent setups under different optical densities as

shown in Fig. 4. Once light was switched on, electrodes immediately collected charge carriers. While the falling edges were a little bit slow, the photocurrent still can fall back to the lower level within  $2\mu\text{s}$ . Although the capacitive current was strong and fluctuated the output current, it is worth mentioning that photocurrent responsivity under different light intensities showed a similar decay curve up to the microsecond time domain. This intensity independence most probably suggests photocurrent signal was detectable in low light condition.

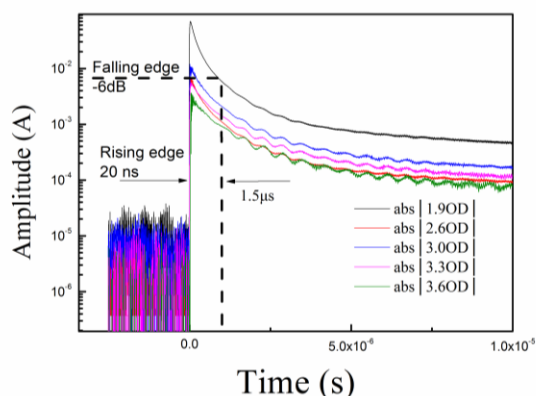


Fig. 4. Photocurrent decay under different light irradiation intensity, the y axis was plotted after logarithm operation

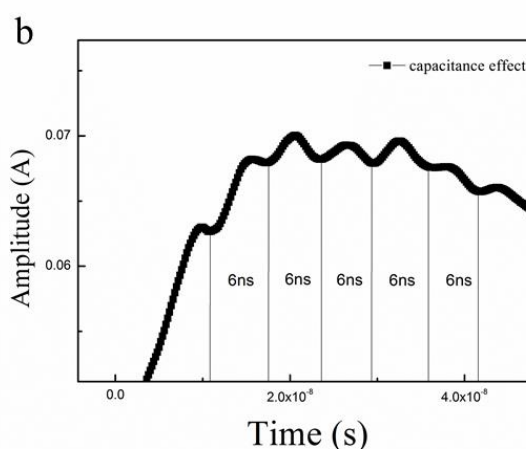
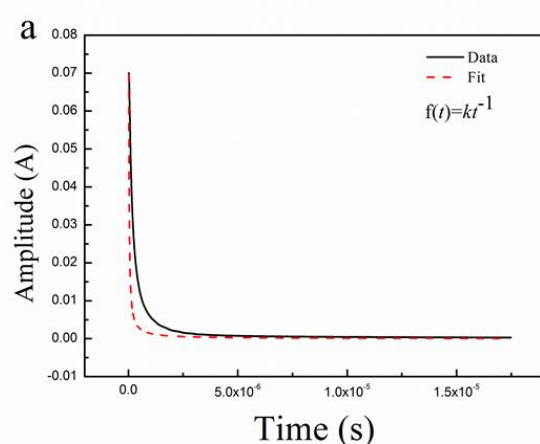


Fig. 5. (a) Photocurrent decay curve fitted with geminate recombination, (b) shows the capacitance effect inside of BHJ, the oscillation period was around 6 ns

#### 4. Conclusion

A potential application of organic semiconductors has been demonstrated as photo sensor based on P3HT: PCBM bulk heterojunction. The photodetector stable worked under different light intensity. In order to eliminate the effect from dark current, Photodetector was driven at a reverse bias voltage of  $-2.5\text{ V}$ . The organic sensor demonstrated a rapid response in microsecond scale under different irradiation intensity. Contrast with silicon diodes, though the response wavelength was only around  $550\text{ nm}$ , the stable performance already has demonstrated a

potential application in future sensing market. As we assumed that geminate recombination dominated the decay process, the curve was then fitted by the recombination rate which got from TAS background, the fitted curve was shown in Fig. 5a. Though we mentioned that geminate recombination dominated the decay process, the original curve decay obviously slower than the fitted curve. This phenomenon was caused by electrodes because built-in electric field [31] could extract charge carriers to each side respectively. Contrast with naked BHJ films, parts of charge carriers stayed close to electrodes instead of remaining around the D/A interface. As a result, the decay rate was slower than pure geminate recombination process. Meanwhile, after charge extraction, the capacitance forms because fabrication methods and charge depletion. In our sample, a faradic oscillation period was around  $6\text{ ns}$  as shown in Fig. 5b. compares to  $1.5\text{ to }2\mu\text{s}$  response time, the faradic oscillation was much fast which can be neglected in future applications. For further circuit design, the capacitance would have a significant impact on circuit. In this article, the capacitance of OPD was around  $8.14\mu\text{F}$  according to RC calculation which is close to conventional silicon photodetectors.

potential application in future sensing market.

#### Acknowledgement

This work was granted by the Doctor Candidate Foundation of Jiangnan University (JUDCF13039). The authors thank the grant from the Education Department of Jiangsu Province, China (CXZZ13\_0742). Thanks for the funding from industry university research projects of Jiangsu Province (BY2015019-04).

## References

- [1] H. Hoppe, N. S. Sariciftci, *Journal of Materials Research* **19**(7), 1924 (2004).
- [2] P. A. Yakimov, S. R. Forrest, *Journal of Applied Physics* **93**(71), 3693 (2003).
- [3] C. W. Tang, S. A. Vanslyke, *Applied Physics Letters* **51**(12), 913 (1987).
- [4] H. M. Zeyada, M. M. El-Nahass, M. M. El-Shabaan, *Synthetic Metals* **220**, 102 (2016).
- [5] Z. L. Yuan, M. X. Fu, Y. J. Ren, W. D. Huang, C. J. Shuai, *Microelectronic Engineering* **163**, 32 (2016).
- [6] J. S. Yu, Y. F. Zheng, J. Huang, *Polymers* **6**(9), 2473 (2014).
- [7] B. K. Sharma, J. H. Ahn, *Advanced Electronic Materials* **2**(8), 1600105 (2016).
- [8] J. C. Wang, X. J. Zhang, W. Deng, Q. X. Shang, L. Wang, L. B. Zhong, *Organic Electronics* **34**, 104 (2016).
- [9] Z. F. An, C. Zheng, Y. Tao, R. F. Chen, H. F. Shi, T. Chen, Z. X. Wang, H. H. Li, R. R. Deng, X. G. Liu, *Nature Materials* **14**, 685 (2015).
- [10] R. Shiwaku, Y. Takeda, T. Fukuda, K. Fukuda, H. Matsui, D. Kumaki, S. Tokito, *Scientific Reports* **6**, 34723 (2016).
- [11] C. W. Liu, M. H. Lee, M. J. Chen, I. C. Lin, C. F. Lin, *Applied Physics Letters* **76**(12), 1516 (2000).
- [12] H. C. Card, E. H. Rhoderick, *Journal of Physics D: Applied Physics* **10**, 1589 (1971).
- [13] P. Buzhan, B. Dolgoshein, A. Llyin, V. Lamtsеров, V. Kaplin, A. Karakash, L. Filatov, *ICFA Inst. Bull.* **21**, 28 (2001).
- [14] H. Yao, L. Ye, H. Zhang, S. Li, S. Zhang, J. Hou, *Chemical Reviews* **116**(12), 7397 (2016).
- [15] H. Thomas, R. M. William, D. Andreas, F. F. Urs, C. Rongrong, H. N. William, B. Markus, S. Michael, V. D. Max, H. G. Efelhaaf, M. D. McGehee, C. G. Brabec, *Energy and Environmental Science* **9**, 247 (2016).
- [16] A. Rizzo, A. Cester, N. Warchien, N. Lago, L. Torto, M. Barbato, J. Favaro, S. E. A. Gevorgyan, M. Corazza, F. C. Krebs, *Solar Energy Materials and Solar Cells* **157**, 337 (2016).
- [17] Y. Y. Zhang, A. M. Wang, X. J. Tian, Z. J. Wen, H. J. Lv, D. S. Li, J. Y. Li, *Journal of Hazardous Materials* **318**, 319 (2016).
- [18] L. Tayadakov, K. Lyssenko, R. Saifutyarov, A. Akkuzina, R. Avetisov, A. Mozhevitina, I. Avetissov, *Dyes and Pigments* **135**, 80 (2016).
- [19] A. C. Wei, J. R. Sze, *Optics Communications* **380**, 394 (2016).
- [20] Y. Kang, B. Yuan, D. J. Zhang, T. Ma, X. C. Huang, Z. Y. Chu, K. Lai, *Journal of Luminescence* **179**, 501 (2016).
- [21] S. S. Reddy, W. Cho, V. G. Sree, S. H. Jin, *Dyes and Pigments* **134**, 315 (2016).
- [22] S. B. Lim, C. H. Ji, K. Y. Kim, S. Y. Oh, *Journal of the Korean Physical Society* **69**, 421 (2016).
- [23] S. H. Kim, S. Heo, D. J. Yun, R. Satoh, G. Park, K. S. Kim, *Japanese Journal of Applied Physics* **55**, 091601 (2016).
- [24] T. N. Ng, W. S. Wong, M. L. Chabinye, S. Sambandan, R. A. Street, *Applied Physics Letters* **92**(21), 213303 (2008).
- [25] B. Arredondo, C. D. Dios, R. Vergaz, G. D. Pozo, B. Romero, *IEEE Photonics Technology Letters* **24**(20), 1868 (2012).
- [26] N. M. Abd-Alghafour, N. M. Ahmed, Z. Hassan, M. Bououdina, *Applied Physics A-Materials Science and Processing*, **122**, 817 (2016).
- [27] S. L. Tan, X. Y. Zhao, K. L. Chen, K. B. Crozier, Y. P. Dan, *Applied Physics Letters* **109**(3), 033505 (2016).
- [28] X. Xi, X. J. Chen, S. Zhang, W. J. Li, Z. R. Shi, G. H. Li, *Solar Energy* **114**, 198 (2015).
- [29] G. Juska, K. Genevicius, N. Nekrasas, R. Osterbacka, *Applied Physics Letters* **95**(1), 013303 (2009).
- [30] A. Pivrikas, N. S. Sariciftci, G. Juška, R. Österbacka, *Progress in Photovoltaics: Research and Applications* **15**(8), 677 (2007).
- [31] C. G. Shuttle, B. O'Regan, A. M. Ballantyne, J. Nelson, D. D. C. Bradley, J. C. D. Mello, J. R. Durrant, *Applied Physics Letters* **91**, 093311 (2008).
- [32] E. Klimov, W. Li, X. Yang, G. G. Hoffmann, J. Loos, *Macromolecules* **39**(13), 4493 (2006).

\*Corresponding author: water198966@hotmail.com